PHOTONIC SENSORS / Vol. 12, No. 3, 2022: 220308

Alternative Interpretation of Speckle Autocorrelation Imaging Through Scattering Media

Honglin LIU[1*], Puxiang LAI[2,3*], Jingjing GAO[1], Zhentao LIU[1], Jianhong SHI[4], and Shensheng HAN[1,5]

[1]*Key Laboratory for Quantum Optics, Shanghai Institute of Optics and Fine Mechanics, Chinese Academy of Sciences, Shanghai 201800, China*

[2]*Department of Biomedical Engineering, The Hong Kong Polytechnic University, Hong Kong, China*

[3]*Hong Kong Polytechnic University Shenzhen Research Institute, Shenzhen 518000, China*

[4]*State Key Laboratory of Advanced Optical Communication Systems and Networks and Center of Quantum Sensing and Information Processing (QSIP), Shanghai Jiao Tong University, Shanghai 200240, China*

[5]*Hangzhou Institute for Advanced Study, University of Chinese Academy of Sciences, Hangzhou 310024, China*

[*]Corresponding authors: Honglin LIU and Puxiang LAI E-mails: hlliu4@hotmail.com and puxiang.lai@polyu.edu.hk

Abstract: High-resolution optical imaging through or within thick scattering media is a long sought after yet unreached goal. In the past decade, the thriving technique developments in wavefront measurement and manipulation do not significantly push the boundary forward. The optical diffusion limit is still a ceiling. In this work, we propose that a scattering medium can be conceptualized as an assembly of randomly packed pinhole cameras and the corresponding speckle pattern as a superposition of randomly shifted pinhole images. The concept is demonstrated through both simulation and experiments, confirming the new perspective to interpret the mechanism of information transmission through scattering media under incoherent illumination. We also analyze the efficiency of single-pinhole and dual-pinhole channels. While in infancy, the proposed method reveals a new perspective to understand imaging and information transmission through scattering media.

Keywords: Imaging; scattering media; pinhole; information channel; autocorrelation; transport mean free path; random phasemask

Citation: Honglin LIU, Puxiang LAI, Jingjing GAO, Zhentao LIU, Jianhong SHI, and Shensheng HAN, "Alternative Interpretation of Speckle Autocorrelation Imaging Through Scattering Media," *Photonic Sensors*, 2022, 12(3): 220308.

Open Science Identity (OSID)

1. Introduction

Optical imaging through scattering media is highly desired yet unresolved, especially when the medium is thick. For decades, researchers struggle to see deeper or thicker while maintaining high resolution. Unfortunately, the tradeoff between the thickness and resolution is still unbroken, even after recent thriving developments in optical phase conjugation [1–7], wavefront shaping [8–14], scattering matrix measurement [15–19], hybrid acousto-optical methods [3, 4, 13, 20–24], etc. Most

Received: 19 September 2021 / Revised: 22 December 2021

DOI: 10.1007/s13320-022-0654-9
Article type: Regular

proof-of-concept implementations thus far have dealt with thin scattering media, such as ground glass diffusers, painting power layers, and thin biological tissue slices, which can hardly be extended to thick scattering media. A possible reason behind the dilemma is that all these methods treat a scattering medium as a black box, where only the input(s) and output(s) of the medium are considered but the medium itself is not. Yet, the essence of imaging is to transmit information. In information theory, the concept of channel is widely explored to transmit information faster and farther after the popularity of data compression and source coding [25]. However, as the thickness of scattering media increases, the imaging quality deteriorates rapidly. To understand and furtherly tackle the poor information transmission efficiency, the concept of channel for information delivery in scattering media needs to be amended.

Among all the solutions to imaging through scattering media, speckle autocorrelation imaging [26–34] is attractive due to its plain experiment implementation. Its principle is also quite straight forward. Under incoherent illumination, the resultant speckle pattern on the detection plane is a convolution of a hidden object and a speckle point spread function (sPSF) of the medium, if the object is smaller than the memory effect range [35–39]. Under ensemble average approximation, the autocorrelation of speckles equals to the autocorrelation of the object itself, thus the image can be reconstructed based on algorithms [25, 40–43]. With further scrutinization, we find that a scattering medium can be conceptually treated as an array of randomly distributed fictitious pinholes and the corresponding speckle pattern as a superposition of randomly shifted pinhole images. It is hence hypothesized that pinholes constitute major channels to transmit information through scattering media, which is demonstrated via both simulation and experiments in this work. In the following, we first simulate amplitude pinholes on a screen, then build a phase pinhole model considering that most light is scattered rather than blocked or absorbed in scattering media, and finally extend the simulation to three dimensions with phase pinholes being positioned on several sequential planes. Experimental results confirm that randomly packed phase pinholes provide open channels to transmit information through thick scattering media, and furtherly single-pinhole channels are more efficient than dual-pinhole channels for information transmission.

2. Methods

In speckle autocorrelation imaging, the speckle pattern on the image plane can be denoted by [25]

$$I(x', y') = O(x', y') \otimes \mathrm{sPSF} \tag{1}$$

within the memory effect range, where $\otimes$ is the convolution operator, and sPSF denotes the speckle PSF of the scattering medium. O is an intensity object, and x and y denote the coordinates on the image plane. The autocorrelation of the speckle pattern can be

$$\begin{aligned} I(x', y') * I(x', y') &= \left[O(x', y') * O(x', y')\right] \otimes \\ &\quad \left[\mathrm{sPSF} * \mathrm{sPSF}\right] \\ &\cong O(x', y') * O(x', y') \end{aligned} \tag{2}$$

where $*$ is the autocorrelation operator. $\mathrm{sPSF} * \mathrm{sPSF}$ can be considered as a pink function. After Fourier transform, (2) turns to be

$$\left|\tilde{F}\left[I(x', y')\right]\right| = \left|\tilde{F}\left[O(x', y')\right]\right|. \tag{3}$$

In other words, the Fourier transforms of the intensity object and its corresponding speckle pattern share the same amplitude distribution in the frequency domain.

In the pinhole image, the intensity distribution on the image plane is

$$\begin{aligned} I(x', y') &= \iint O(x, y)\,\delta(x + x', y + y')\,\mathrm{d}x\mathrm{d}y \\ &= O(-x', -y') \end{aligned} \tag{4}$$

where $O(x, y)$ is the intensity distribution of the object on the object plane, and $\delta(x + x', y + y')$ is

the ideal response function of the pinhole camera. The case of equal object and image distances is selected to simplify the derivation following. Equation (4) has another form:

$$I(x', y') = [O \otimes \delta](x', y') \tag{5}$$

where $\delta(x', y')$ is the point spread function. Under geometric assumption, the diameter of the pinhole is zero. If the center of the pinhole is shifted to (x_p, y_p), the corresponding PSF is $\delta(x'-2x_p, y'-2y_p)$, and (5) turns to be

$$I(x', y') = O(x', y') \otimes \delta(x'-2x_p, y'-2y_p). \tag{6}$$

Then, the autocorrelation of the pinhole image is

$$\begin{aligned} & I(x', y') * I(x', y') \\ &= \left[O(x', y') \otimes \delta(x'-2x_p, y'-2y_p)\right] * \\ &\quad \left[O(x', y') \otimes \delta(x'-2x_p, y'-2y_p)\right] \\ &= \left[O(x', y') * O(x', y')\right] \otimes \\ &\quad \left[\delta(x'-2x_p, y'-2y_p) * \right. \\ &\quad \left. \delta(x'-2x_p, y'-2y_p)\right] \\ &= \left[O(x', y') * O(x', y')\right] \otimes \delta(x', y') \\ &= O(x', y') * O(x', y'). \end{aligned} \tag{7}$$

No matter where the center is, the autocorrelation of each pinhole image is the same and can be added directly. Considering a screen with many randomly distributed pinholes, the intensity on the image plane is

$$\begin{aligned} I(x', y') &= \sum_i O(x', y') \otimes \delta(x'-2x_{pi}, y'-2y_{pi}) \\ &= O(x', y') \otimes \sum_i \delta(x'-2x_{pi}, y'-2y_{pi}) \end{aligned} \tag{8}$$

where $(x_{pi}, y_{pi})(i = \text{integers})$ is the center of ith pinhole. Because of the zero width of an ideal pinhole, the autocorrelation of $\sum\delta(x'-2x_{pi}, y'-2y_{pi})$ equals $\delta(x', y')$, and the intensity autocorrelation still equals the autocorrelation of the object itself. As the number density of pinholes increases, the intensity on the image plane evolves from sparsely distributed images into a speckle pattern.

Apparently, (1) and (8) have similar forms. In both cases, the autocorrelation of intensity distribution on the image plane equals the autocorrelation of the object itself. Thus, we assume that a scattering medium can be conceptualized as many randomly packed pinholes and the corresponding speckle pattern as a superposition of randomly shifted pinhole images.

To demonstrate the assumption above, based on wave optics we first simulate the detected intensity patterns and reconstruct images using an amplitude pinhole screen, when the number of pinholes is gradually changed. The system setup is shown in Fig. 1. A thermal source at a wavelength of 532 nm illuminates a transmissive object, such as a letter "F", a Greek letter "α", an icon and a digit number "4". The transmitted light propagates to the screen, and finally reaches the camera. The object distance u=8 cm and the image distance v=4 cm. The pinhole diameter is selected as 180 μm. Considering most turbid media of interest (e.g., biological tissue) are scattering dominant, i.e., the scattering coefficient is an order of magnitude larger than the absorption coefficient, we build a model of the phase pinhole, which has higher energy efficiency than the amplitude pinhole. For a thin scattering layer, the decomposed phase pinholes are randomly distributed on a plane; while for a thick scattering medium, it is sliced into many thin layers and each layer is treated as lots of phase pinholes. In this way, we can extend the idea into 3 dimensions. Physically, we cannot decompose a real scattering medium into phase pinholes. Hence, simulation is also applied to demonstrate the hypothesis, as shown in Figs. 3 and 5, since the pinhole decomposition process can be easily implemented conceptually.

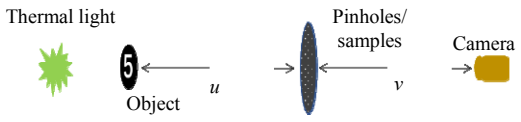

Fig. 1 Configuration of the system in both simulation and experiment. u=8 cm, v=4 cm. In experiment, a light emitting diode (LED) (Thorlabs M530L3) coupled with a 1-nm-linewidth filter is used as the illumination source. The charge-coupled device (CCD) camera (AVT Stinggray F-504B) has a pixel pitch of 3.45 μm.

After the demonstration, it is reasonable to treat pinhole as a kind of channel to transmit information through scattering media, and a scattering medium can be decomposed into numerous pinholes with different diameters, shapes (circular, hexagon, etc.), and clusters. How do these factors influence the channel efficiency/capacity? Many remain to be explored. Here, we only consider a very simple case, comparing the channels constituted by a single pinhole and by two pinholes in sequence. In experiment, we prepare 4 scattering samples, i.e., a single ground glass diffuser (Thorlabs DG20-600-MD), two diffusers with their rough surfaces in direct contact with each other, two diffusers with one A4 paper circle of a thickness around 100 μm as the spacer between the rough surfaces, and two diffusers with two A4 paper circles as the spacer. u and v are the same as the simulation. The measured memory effect range for the latter three cases are 7 089.1 μm, 728.3 μm, and 493.1 μm, respectively. Legends 0A4, 1A4, and 2A4 denote samples with different numbers of A4 spacers. The object digit "4" has a height of 320 μm, smaller than memory effect ranges of all samples. Note that a ground glass diffuser is usually considered to generate one scattering event at its rough surface, and when the two rough surfaces of two ground glass diffusers are in direct contact, the single scattering approximation is still valid. For a single diffuser, all decomposed phase pinholes are located on its rough surface. In this case, the input of all pinholes is the object. Any two pinholes are independent to transmit information with known channel efficiency/capacity unless they have overlaps. The overlap causes crosstalk that brings distortion of the corresponding pinhole images and hence noise to deteriorate the quality of reconstructed images. While in the two-diffuser sample with large intervals, each diffuser is decomposed into many phase pinholes. Two pinholes located respectively on the two diffusers constitute the dual-pinhole channel, whose capacity/efficiency to transmit information is determined by pinhole diameters, interval distance and central shift. The overlap between two dual-pinhole channels also brings noise. To scrutinize the efficiency of the two channels, we also do simulations based on dual-phasemask samples with different intervals.

3. Results

Figure 2 shows the simulation results of a screen with an increased number of amplitude pinholes. As seen, with sparse pinholes (e.g., N=20), the images on the CCD plane are clearly distinguishable [Fig. 2(b)], and the digit image can be reconstructed. When the number of pinholes increases [Figs. 2(d), 2(g), and 2(j)], more and more images are superposed, resulting in more and more speckles like patterns [Figs. 2(e), 2(h), and 2(k)]. But with retrieval algorithms [25, 34], the digit can still be reconstructed [Figs. 2(f), 2(i), and 2(l)], albeit with increased noise caused by the truncations of four edges of the speckle patterns and the crosstalk among overlapping pinholes.

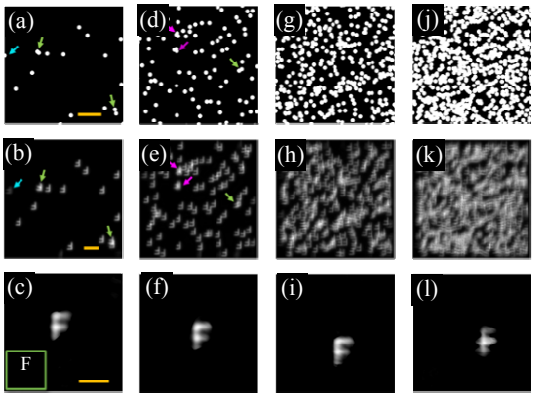

Fig. 2 Simulation of pinhole camera imaging through different amplitude pinhole screens. The first row is the simulated distributions of the pinholes on the screen, the second and thirds rows show the corresponding light patterns on the camera and reconstructed images, respectively. The number of pinholes gradually increases from column to column (N=20, 100, 400, and 900). The scale bars of the three rows are 1 mm, 1 mm, and 0.5 mm, respectively. The inset in (c) is the photograph of the object, i.e., a hollowed letter F. The colored arrows in the first and second rows attract attentions to particular pinholes and their corresponding pinhole images.

The azure arrow in Fig. 2(a) shows a half pinhole of a semi-circle, and its pinhole image in Fig. 2(b) is dimmer than the regular pinhole images. The three green arrows in Figs. 2(a) and 2(d) denote two pinholes have overlap, but with different center-to-center distances, and their corresponding

images have different profiles. The magenta arrows show two different clusters of three pinholes, and the corresponding images also have different shapes.

Figure 3 is the simulation result of the phase pinhole camera concept. First, a phase pinhole is designed by positioning a small phase disk on a transparent plate. A reversed image of the Greek letter α can be obtained (shown in the second row), as long as the phase value of the disk is not the same as or $2n\pi$ (n is an integer) different from that of the background. The result demonstrates that under incoherent illumination, phase pinholes can be used for imaging, albeit seeming counter-intuitive. Notably, the background of the light pattern reaching the detection plane is bright, which is different from amplitude pinholes. As the number density increases, more and more phase pinholes overlap. In other words, a point can be the component of many decomposed pinholes simultaneously. Thus, the diffraction light of a point is decomposed into different pinhole cameras. An example of a phasemask generated from plenty of packed phase pinholes and the corresponding speckle pattern are shown in Figs. 3(f) and 3(g). Nevertheless, an image of the object can still be extracted [Fig. 3(h)]. The results demonstrate that a thin scattering medium can be decomposed as randomly distributed phase pinholes.

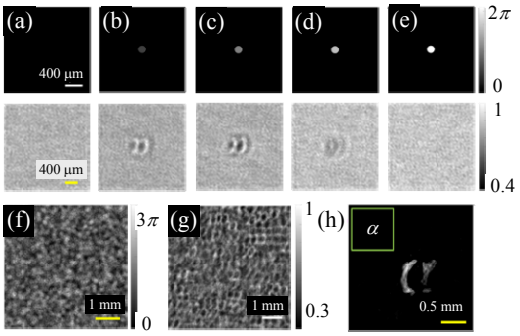

Fig. 3 Simulation results of randomly packed phase pinhole cameras: (a)–(e) the upper row illustrates phase screens with only one circular bump of uniform phase (0, $\pi/2$, π, $3\pi/2$, and 2π, respectively) at the center; the lower row is the corresponding intensity patterns on the detection plane; (f) an example of phase screen with 10^4 randomly distributed phase bumps within a field of view of 5×5 mm^2. The phase step height of each pinhole is $\pi/8$; (g) the corresponding light pattern after normalization; (h) the reconstructed image.

In addition to circles, the phase pinhole can have other distributions, such as Gaussian profiles. As shown in Fig. 4, enough randomly distributed Gaussian phase pinholes within an area share the same statistical distribution as a ground glass model, a typical thin scattering medium. One more evidence to show that a scattering medium can be decomposed into randomly shifted phase pinholes. Now, the concept has been well demonstrated with the thin scattering medium. For a thick scattering medium, such as a 1-mm-thick layer of chicken breast tissue, it can be sliced into 10 100-μm-thick layers, and each layer is replaced by many Gaussian phase pinholes. The icon is selected as the target, with simulation result shown in Fig. 5. Due to the increased noise, and maybe also the decreased capacity/efficiency of the integrated channels, the reconstructed image is poor. Nevertheless, we can still see the profile of the target. It demonstrates that the pinhole camera concept can be applied to thick scattering media as well.

Figure 6 shows the imaging results of channels constituted by single-pinhole and dual-pinhole in comparison. As the distance between the rough surfaces increases, the single scattering approximation gradually fails, and more edge information in the speckle autocorrelation is lost [Fig. 6(b) to 6(e)]. We can barely reconstruct the image for the fourth scattering medium although the object is still within the memory effect range. To avoid the influence of noise in detection and further confirm the efficiency of the two channels to transmit information, we design a simulation accordingly, where the weight of zero frequency component is adjustable [39, 44–46]. We record the speckle patterns of a single phasemask and two phasemasks separated by 10 μm, 100 μm, and 1 000 μm, respectively. Their autocorrelations are shown in Figs. 6(f) to 6(i). Compared with the autocorrelation of the object in Fig. 6(a), the speckle autocorrelation, especially in the edge, deteriorates with increased intervals [Figs. 6(g) to 6(i)]. It suggests that even within the memory effect range, the single-pinhole channel has higher capacity/efficiency to transmit information. By adding a little

bit ballistic photons (0.18%, counted by power/energy) to the optical field of the first phasemask of the two-phasemask sample, accordingly 0.18% increment of single-pinhole channels to the sample, speckle autocorrelation can be significantly improved as shown in Fig. 6(j), which can also be seen in Fig. 6(k) from the structural similarity (SSIM).

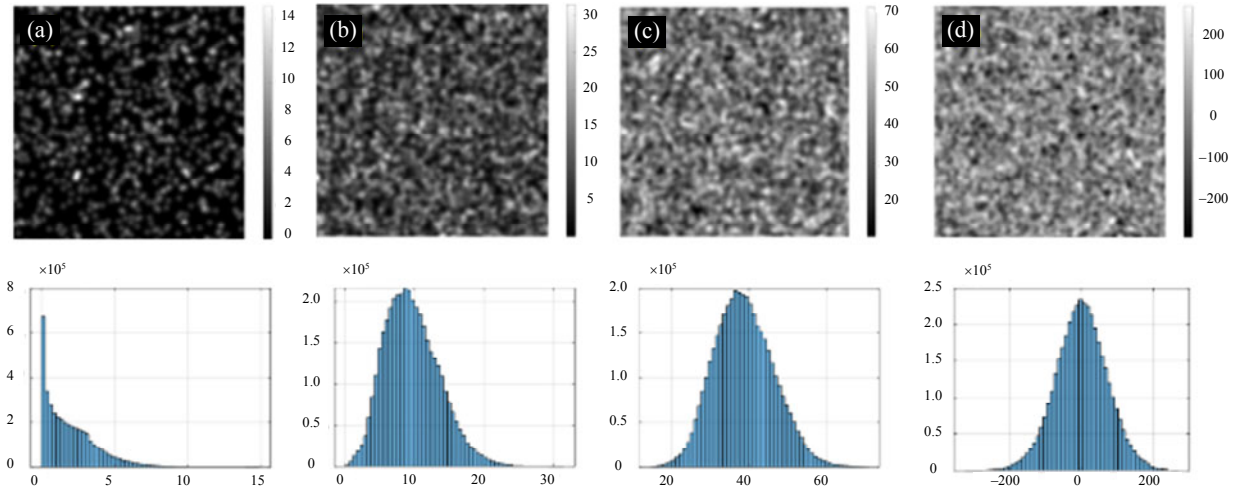

Fig. 4 Evolution of phasemasks with the number of Gaussian bumps with a height of π and a radius κ=60 μm. Within a 2×2 mm^2 square area, 10^3, 5×10^3, and 2×10^4 Gaussian phase pinholes are randomly distributed in the upper row of (a–c), respectively. The colorbars denote phase value range of generated phasemasks accordingly. (d) A conventional phasemask generated under the constraint $G(x,y)=\sigma^2\exp[-(x^2+y^2)/\kappa^2]$ at σ =10 μm and κ =60 μm, corresponding to a Gaussian filter in frequency domain. As the phasemask grows maturely with a nearly symmetric histogram, it has the same appearance and statistical distribution as the conventional one except for the particular phase amplitude, which can be adjusted by adding $2n\pi$, n is an integer. By changing the height and/or number density of the phase pinholes, the phase amplitude and distribution of the generated phasemask can be altered. The vertical axis of the histogram denotes the number of pixels at each phase value.

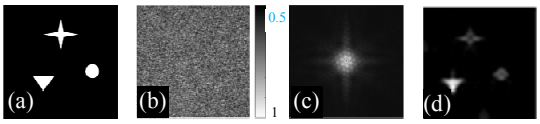

Fig. 5 Simulation result of imaging an icon through a 1-mm-thick layer of chicken breast tissue: (a) a photograph of the icon composed by three geometry structures, (b) and (c) speckle pattern and the amplitude of its Fourier transform, and (d) reconstructed image of the icon.

4. Discussion and conclusions

In this paper, for simplification we assume that pinholes have the same shape and diameter in each decomposition. In fact, both the shapes and the diameters of pinholes can be different, as well as the heights. In other words, the decomposition of a scattering medium is not unique. However, the image result, which is an ensemble average, is the same. In different compositions, the quality of a particular pinhole image is different, but not the ensemble average.

Comparing to fog and clouds, the pinhole concept is more applicable in dense scattering media, such as biological tissue, turbid solution, and epoxy

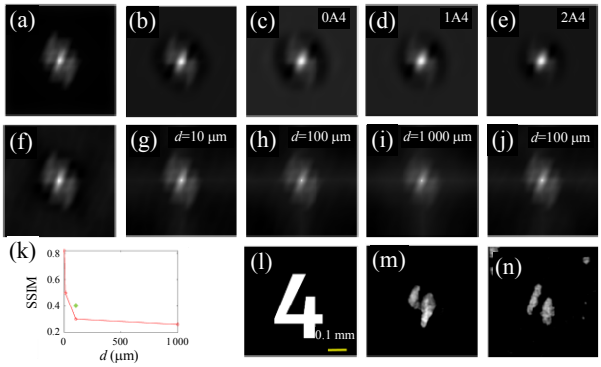

Fig. 6 Experimental and simulated results of single- and dual-pinhole channels to transmit information: (a) the autocorrelation of the target; (b)–(e) the speckle autocorrelation of the prepared scattering media, i.e., a single diffuser, dual diffusers with 0, 1 and 2 A4 paper circles as the spacer, respectively; (f)–(i) the normalized speckle autocorrelation of a single phasemask, dual phasemasks with intervals of 10 μm, 100 μm, and 1 000 μm, respectively. As the interval increases, the distortion of the edge increases; (j) the speckle autocorrelation with 100 μm interval when 0.18% ballistic, i.e., zero frequency component is added to the spatial power spectrum density of the first phasemask; (k) the structural similarity (SSIM) of simulated autocorrelations with the autocorrelation of object itself. With increased single channels to transmit information, the SSIM value increases at the same interval of d=100 μm, as denoted by the green diamond marker; (l) the photograph of the target with a scale bar of 100 μm; (m) the reconstructed image from the speckle pattern obtained in experiment at d=100 μm; (n) the reconstructed image from corresponding simulation pattern.

resin plates. For much larger scale media, like dense fog, although they can also be considered as stacks of random phase masks with intervals as well, the memory effect range is almost zero due to tens of hundreds of meters or even larger scales. In these cases, images cannot be retrieved even when speckle patterns are obtained.

For a long time, the community has been striving to overcome the barrier of multiple scattering to see and manipulate light through/within thick scattering media. Although many techniques have been developed to advance the frontier, the imaging depth/thickness is still limited, usually within one transport mean free path beneath surface. The ceiling is there; it seems that technique improvements in devices like cameras, spatial light modulators will not change the situation fundamentally. So, instead of treating a scattering medium as a black box and only probing the inputs and outputs, looking into scattering media from the perspective of field and information propagation may potentially pave a new avenue to the ultimate solution.

In this work, a new concept is proposed and demonstrated to treat the scattering medium as an assembly of randomly packed pinhole cameras in 3D space and the speckle pattern as a superposition of numerous pinhole images with randomly shifted centers. Moreover, an interpretation of information delivery through a scattering medium is shown that singly scattered photons are the major carriers for effective image information and pinholes provide open channels for information transmission, or equivalently, the single-pinhole channel has higher efficiency/capacity to transmit information. That said, for now merely a peek of the channel to transmit information in scattering media and only the ensemble average of single-pinhole and dual-pinholes channels, not each particular form, have been investigated. With further research, we may find many more sophisticated channels, which have a comprehensive understanding of the channels in scattering media, manipulate the channel to increase information transmission efficiency, and pave a new avenue to image through thick scattering media. The study may find immediate and future benefits to a variety of applications in complex environment, such as quantitative biological fluorescence imaging, precise treatment planning, and navigation in fog.

Acknowledgement

The authors thank Dr. Lihong V. Wang for inspiring and helpful discussions. This work was supported by the National Key Research and Development Program of China (Grant No. 2016YFC0100602), National Natural Science Foundation of China (Grant Nos. 81930048, 81671726, and 81627805), Guangdong Science and Technology Commission (Grant Nos. 2019BT02X105, and 2019A1515011374), Hong Kong Research Grant Council (Grant Nos. 15217721, R5029-19, and C7074-21GF), and Hong Kong Innovation and Technology Commission (Grant Nos. GHP/043/19SZ and GHP/044/19GD).

References

[1] Z. Yaqoob, D. Psaltis, M. S. Feld, and C. Yang, “Optical phase conjugation for turbidity suppression in biological samples,” *Nature Photonics*, 2008, 2(2): 110–115.

[2] S. Farahi, G. Montemezzani, A. A. Grabar, J. P. Huignard, and F. Ramaz, “Photorefractive acousto-optic imaging in thick scattering media at 790 nm with a $Sn_2P_2S_6$:Te,” *Optics Letters*, 2010, 35(11): 1798–1800.

[3] X. Xu, H. Liu, and L. V. Wang, “Time-reversed ultrasonically encoded optical focusing into scattering media,” *Nature Photonics*, 2011, 5(3): 154–157.

[4] Y. M. Wang, B. Judkewitz, C. A. Di Marzio, and C. Yang, "Deep-tissue focal fluorescence imaging with digitally time-reversed ultrasound encoded light," *Nature Communications*, 2012, 3(1): 1–8.

[5] Y. Liu, C. Ma, Y. Shen, J. Shi, and L. V. Wang, "Focusing light inside dynamic scattering media with millisecond digital optical phase conjugation," *Optica*, 2017, 4(2): 280–288.

[6] G. Pang, H. Liu, P. Hou, M. Qiao, and S. Han, "Optical phase conjugation of diffused light with infinite gain by using gated two-color photorefractive crystal $LiNbO_3$:Cu:Ce," *Applied Optics*, 2018, 57(10): 2675–2678.

[7] J. Ryu, M. Jang, T. J. Eom, C. Yang, and E. Chung, "Optical phase conjugation assisted scattering lens: variable focusing and 3D patterning," *Scientific Reports*, 2016, 6(1): 1–8.

[8] I. M. Vellekoop and A. P. Mosk, "Focusing coherent light through opaque strongly scattering media," *Optics Letters*, 2007, 32(16): 2309–2311.

[9] N. Ji, D. E. Milkie, and E. Betzig, "Adaptive optics via pupil segmentation for high-resolution imaging in biological tissues," *Nature Methods*, 2010, 7(2): 141–147.

[10] D. Akbulut, T. J. Huisman, E. G. Van Putten, W. L. Vos, and A. P. Mosk, "Focusing light through random photonic media by binary amplitude modulation," *Optics Express*, 2011, 19(5): 4017–4029.

[11] R. Fiolka, K. Si, and M. Cui, "Complex wavefront corrections for deep tissue focusing using low coherence backscattered light," *Optics Express*, 2012, 20(15): 16532–16543.

[12] R. Horstmeyer, H. Ruan, and C. Yang, "Guidestar-assisted wavefront-shaping methods for focusing light into biological tissue," *Nature Photonics*, 2015, 9(9): 563–571.

[13] P. Lai, L. Wang, J. W. Tay, and L. V. Wang, "Photoacoustically guided wavefront shaping for enhanced optical focusing in scattering media," *Nature Photonics*, 2015, 9(2): 126–132.

[14] H. Yu, J. Park, K. Lee, J. Yoon, K. Kim, S. Lee, *et al.*, "Recent advances in wavefront shaping techniques for biomedical applications," *Applied Physics*, 2015, 15(5): 632–641.

[15] S. M. Popoff, G. Lerosey, R. Carminati, M. Fink, A. C. Boccara, and S. Gigan, "Measuring the transmission matrix in optics: an approach to the study and control of light propagation in disordered media," *Physical Review Letters*, 2010, 104(10): 100601.

[16] H. Yu, T. R. Hillman, W. Choi, J. O. Lee, M. S. Feld, R. R. Dasari, *et al.*, "Measuring large optical transmission matrices of disordered media," *Physical Review Letters*, 2013, 111(15): 153902.

[17] A. Goetschy and A. D. Stone, "Filtering random matrices: the effect of incomplete channel control in multiple scattering," *Physical Review Letters*, 2013, 111(6): 063901.

[18] Y. Choi, T. R. Hillman, W. Choi, N. Lue, R. R. Dasari, P. T. C. So, *et al.*, "Measurement of the time-resolved reflection matrix for enhancing light energy delivery into a scattering medium," *Physical Review Letters*, 2013, 111(24): 243901.

[19] M. Kim, W. Choi, Y. Choi, C. Yoon, and W. Choi, "Transmission matrix of a scattering medium and its applications in biophotonics," *Optics Express*, 2015, 23(10): 12648–12668.

[20] E. Zhang, J. Laufer, R. Pedley, and P. Beard, "In vivo high-resolution 3D photoacoustic imaging of superficial vascular anatomy," *Physics in Medicine & Biology*, 2009, 54(4): 1035.

[21] X. Xu, S. R. Kothapalli, H. Liu, and L. V. Wang, "Spectral hole burning for ultrasound-modulated optical tomography of thick tissue," *Journal of Biomedical Optics,* 2010, 15(6): 066018.

[22] L. V. Wang and S. Hu, "Photoacoustic tomography: in vivo imaging from organelles to organs," *Science*, 2012, 335(6075): 1458–1462.

[23] Z. Chen, S. Yang, and D. Xing, "Optically integrated trimodality imaging system: combined all-optical photoacoustic microscopy, optical coherence tomography, and fluorescence imaging," *Optics Letters*, 2016, 41(7): 1636–1639.

[24] W. Song, Q. Xu, Y. Zhang, Y. Zhan, W. Zheng, and L. Song, "Fully integrated reflection-mode photoacoustic, two-photon, and second harmonic generation microscopy in vivo," *Scientific Reports*, 2016, 6(1): 1–8.

[25] Aftab, Cheung, Kim, Thakkar, Yeddanapudi, "Information theory & the digital revolution," 6.933 Project History, Massachusetts Institute of Technology, SNAPES@MIT. EDU.

[26] J. Bertolotti, E. G. van Putten, C. Blum, A. Lagendijk, W. L. Vos, and A. P. Mosk, "Non-invasive imaging through opaque scattering layers," *Nature*, 2012, 491(7423): 232–234.

[27] O. Katz, P. Heidmann, M. Fink, and S. Gigan, "Non-invasive single-shot imaging through scattering layers and around corners via speckle correlations," *Nature Photonics*, 2014, 8(10): 784–790.

[28] M. Cua, E. Zhou, and C. Yang, "Imaging moving targets through scattering media," *Optics Express*, 2017, 25(4): 3935–3945.

[29] W. Yang, G. Li, and G. Situ, "Imaging through scattering media with the auxiliary of a known reference object," *Scientific Reports*, 2018, 8(1): 1–7.

[30] C. Guo, J. Liu, T. Wu, L. Zhu, and X. Shao, "Tracking moving targets behind a scattering medium via speckle correlation," *Applied Optics*, 2018, 57(4): 905–913.

[31] H. Liu, X. Wang, J. Gao, T. Yu, and S. Han, "Seeing

through dynamics scattering media: Suppressing diffused reflection based on decorrelation time difference," *Journal of Innovative Optical Health Sciences*, 2019, 12(04): 1942001.

[32] C. Guo, J. Liu, W. Li, T. Wu, L. Zhu, J. Wang, *et al.*, "Imaging through scattering layers exceeding memory effect range by exploiting prior information," *Optics Communications*, 2019, 434: 203–208.

[33] X. Wang, X. Jin, J. Li, X. Lian, X. Ji, and Q. Dai, "Prior-information-free single-shot scattering imaging beyond the memory effect," *Optics Letters*, 2019, 44(6): 1423–1426.

[34] M. Chen, H. Liu, Z. Liu, P. Lai, and S. Han, "Expansion of the FOV in speckle autocorrelation imaging by spatial filtering," *Optics Letters*, 2019, 44(24): 5997–6000.

[35] S. Feng, C. Kane, P. A. Lee, and A. D. Stone, "Correlations and fluctuations of coherent wave transmission through disordered media," *Physical Review Letters*, 1988, 61(7): 834.

[36] I. Freund, M. Rosenbluh, and S. Feng, "Memory effects in propagation of optical waves through disordered media," *Physical Review Letters*, 1988, 61(20): 2328.

[37] S. Schott, J. Bertolotti, J. Léger, L. Bourdieu, and S. Gigan, "Characterization of the angular memory effect of scattered light in biological tissue," *Optics Express*, 2015, 23(10): 13505–13516.

[38] J. Yang, J. Li, S. He, and L. V. Wang, "Angular-spectrum modeling of focusing light inside scattering media by optical phase conjugation," *Optica*, 2019, 6(3): 250–256.

[39] H. Liu, Z. Liu, M. Chen, S. Han, and L. V. Wang, "Physical picture of the optical memory effect," *Photonics Research*, 2019, 7(11): 1323–1330.

[40] J. R. Fienup, "Phase retrieval algorithms: a comparison," *Applied Optics*, 1982, 21(15): 2758–2769.

[41] M. R. Teague, "Deterministic phase retrieval: a Green's function solution," *Journal of the Optical Society of America*, 1983, 73(11): 1434–1441.

[42] R. A. Gonsalves, "Phase retrieval and diversity in adaptive optics," *Optical Engineering*, 1982, 21(5): 215829.

[43] A. Walther, "The question of phase retrieval in optics," *Optica Acta: International Journal of Optics*, 1963, 10(1): 41–49.

[44] S. K. Sinha, E. B. Sirota, S. Garoff, and H. B. Stanley, "X-ray and neutron scattering from rough surfaces," *Physical Review B*, 1988, 38(4): 2297.

[45] Y-P. Zhao, I. Wu, C. F. Cheng, U. Block, G. C. Wang, and T. M. Lu, "Characterization of random rough surfaces by in-plane light scattering," *Journal of Applied Physics*, 1998, 84(5): 2571–2582.

[46] J. W. Goodman, "*Introduction to Fourier Optics* (*2nd Edition*)," New York: MC Graw-Hill Company Publishers, 1996: 130.